CMS Physics Analysis Summary

Contact: cms-pag-conveners-heavyions@cern.ch 2018/05/14

Constraints on nuclear parton distributions from W boson production in pPb collisions at $\sqrt{s_{\mathrm{NN}}} = 8.16$ TeV

The CMS Collaboration

Abstract

The production of W bosons has been measured in proton-lead collisions at a nucleon-nucleon center-of-mass energy of $\sqrt{s_{\mathrm{NN}}} = 8.16$ TeV. The measurement of W bosons is performed in the $\mathrm{W} \to \mu\nu_\mu$ channel, using a data sample with integrated luminosity of 173.4 ± 8.7 nb^{-1} collected by the CMS experiment at the CERN LHC. The number of positive and negative W bosons is determined in the muon pseudorapidity region $|\eta_{\mathrm{lab}}| < 2.4$ and transverse momentum $p_{\mathrm{T}}^{\mu} > 25\,\mathrm{GeV}/c$. The W boson differential cross sections, muon charge asymmetry, and the ratios of W boson yields on the p-going over the Pb-going directions are reported as a function of the muon pseudorapidity in the center-of-mass frame. The measurements are compared to the predictions from theoretical calculations based on parton distribution functions (PDF). The results of this analysis favor PDF calculations including nuclear modifications and provide constraints on the nuclear PDF global fits.

1 Introduction

The production of electroweak gauge bosons has long been considered to be a powerful probe of the parton distribution function (PDF) in the proton [1]. Most recent proton PDF sets include W and Z boson production data from the Tevatron and the CERN Large Hadron Collider (LHC) in their global fit analyses [2–4]. Similarly, the measurements of electroweak boson production in proton-nucleus and nucleus-nucleus collisions, available for the first time at the energy of the LHC, provide constraints to nuclear modifications of the PDFs [5–7]. The presence of a nuclear environment modifies the parton densities in the nucleus compared to those in a free nucleon. The nuclear parton distribution functions (nPDFs) are expected to be enhanced (in the so-called anti-shadowing region) for partons carrying a momentum fraction between $5 \times 10^{-2} \lesssim x \lesssim 10^{-1}$, and suppressed (shadowing region) for $x \lesssim 10^{-2}$ [8]. However, due to the more restricted data sets available in nuclear collisions, the nuclear parton densities are still less precise than in the free-proton case. As a consequence, the precision of quantum chromodynamics (QCD) calculations describing hard processes in heavy ion collisions at high energies is currently limited by nPDF uncertainties.

Since W bosons are predominantly produced via $q\bar{q}$ annihilation through $u\bar{d} \rightarrow W^+$ and $d\bar{u} \rightarrow W^-$, they can be used to probe the quark PDFs. Therefore, the nuclear modifications of the quark PDFs are expected to affect the W boson production in proton-lead (pPb) and lead-lead (PbPb) collisions with respect to proton-proton (pp) collisions at the LHC [7]. More precise measurements of the W boson production in nuclear collisions can further improve the phenomenological extraction of nPDFs. In addition, the asymmetries of the individual yields of W^+ and W^- bosons are known to be a sensitive probe of the down-to-up quark PDF ratio [9–11]; consequently it may allow for the flavor decomposition of u and d quark distributions in nuclei [12]. Note that leptonic decays of W bosons offer a cleaner signal than hadronic decays, since lepton measurements are more precise. Another advantage is that any possible effect due to the medium produced in nuclear collisions should be negligible, since leptons do not interact strongly [13, 14].

Measurements of the W boson production in PbPb collisions at a nucleon-nucleon center-of-mass energy of $\sqrt{s_{\mathrm{NN}}}$ =2.76 TeV, presented by the ATLAS [15–17] and CMS [18–20] Collaborations, have shown that the W boson production is essentially not modified by the nuclear medium formed in these collisions. In pPb collisions, measurements of W production at $\sqrt{s_{\mathrm{NN}}} = 5.02$ TeV have been performed by CMS [12], ATLAS [21] and ALICE [22]. The comparison with perturbative QCD predictions favor the calculations including nPDF effects. A similar observation is made from the analysis of Z boson production in pPb collisions at the same energy [23]. These electroweak boson measurements have been used for the first time in a global fit analysis of nPDF sets (EPPS16 [24]). Nevertheless, a hint of an enhancement of the W^- boson production cross section in the most backward region (Pb ion beam direction) showed some tension with theory calculations (with and without nPDF effects), possibly pointing to different nuclear modifications of the up and down quark PDFs [12]. Additional measurements were thus needed in order to clarify the origin of this discrepancy.

This note reports the results of W boson production in pPb collisions at $\sqrt{s_{\mathrm{NN}}} = 8.16$ TeV. The measurement of W bosons has been performed in the semi-muonic channel using pPb data recorded with the CMS detector in 2016, corresponding to a total integrated luminosity of 173.4 ± 8.7 nb^{-1}. This dataset is roughly six times larger than the one available for the previous measurement at 5.02 TeV. This analysis is performed using events required to have a muon with transverse momentum $p_{\mathrm{T}}^{\mu} > 25$ GeV/c and pseudorapidity $|\eta_{\mathrm{lab}}^{\mu}| < 2.4$. The W boson differential cross sections, muon charge asymmetry and W boson forward-backward

ratios are presented as a function of muon pseudorapidity in the center-of-mass frame.

2 Experimental methods

The central feature of the CMS apparatus is a superconducting solenoid of 6 m internal diameter, providing a magnetic field of 3.8 T. Within the solenoid volume are a silicon pixel and strip tracker, a lead tungstate crystal electromagnetic calorimeter (ECAL), and a brass and scintillator hadron calorimeter (HCAL), each composed of a barrel and two endcap sections. Forward calorimeters extend the pseudorapidity coverage provided by the barrel and endcap detectors. The forward hadron (HF) calorimeter uses steel as an absorber and quartz fibers as the sensitive material. The two halves of the HF are located 11.2 m from the interaction region, one on each end, and together they provide coverage in the range $3.0 < |\eta| < 5.2$. They also serve as luminosity monitors. Muons are measured in the pseudorapidity range $|\eta| < 2.4$, with detection planes made using three technologies: drift tubes, cathode strip chambers, and resistive plate chambers. A more detailed description of the CMS detector, together with a definition of the coordinate system used and the relevant kinematic variables, can be found in Ref. [25].

During the data-taking period, the proton beam was initially circulating clockwise in the LHC ring and its direction was reversed to counterclockwise after a data set corresponding to an integrated luminosity of 62.6 nb^{-1} was collected. The beam energies were 6.5 TeV for the protons and 2.56 TeV per nucleon for the lead nuclei [26]. Due to the asymmetric collision system, massless particles produced at a pseudorapidity η_{CM} in the nucleon-nucleon center-of-mass (CM) frame are reconstructed at $\eta_{\text{lab}} = \eta_{\text{CM}} - 0.465$ (clockwise proton beam) and $\eta_{\text{lab}} = \eta_{\text{CM}} + 0.465$ (counterclockwise proton beam) in the laboratory frame. By convention, the proton-going side defines the positive pseudorapidity region (labelled as forward direction), while the Pb-going side defines the negative pseudorapidity region (backward direction). The W boson measurements presented in this note are expressed in terms of muon η^{μ}_{CM}.

The contamination from background events not originating from inelastic hadronic collisions is suppressed by requiring a total energy deposited in at least one tower in both sides of the HF calorimeter larger than 3 GeV/c. Events are also required to have at least one interaction vertex reconstructed using two or more tracks within a distance from the collision point of 25 cm along the beam axis and 2 cm along its transverse plane. The loss of W bosons due to the pPb collision event selection has been determined to be less than 0.2%.

The main signature of the $\text{W} \to \mu\nu_{\mu}$ process is the presence of a high-p_{T} muon. Events of interest for offline analysis are selected using a trigger algorithm [27] requiring the presence of at least one muon candidate of transverse momentum $p_{\text{T}} > 12$ GeV/c. Moreover, to enhance the signal purity [10, 12], the fiducial region of the analysis has been restricted to muons of $p_{\text{T}} > 25$ GeV/c. The muon candidates are reconstructed in CMS with an algorithm that combines the information from the muon detectors and the tracker [28]. Muons are selected by applying the standard tight selection criteria used in Ref. [29]. The particle-flow (PF) algorithm [30] is used to identify the particles in the event.

The PF algorithm aims to reconstruct and identify each individual particle in an event, with an optimized combination of information from the various elements of the CMS detector. The energy of photons is directly obtained from the ECAL measurement, corrected for zero-suppression effects. The energy of electrons is determined from a combination of the electron momentum at the primary interaction vertex as determined by the tracker, the energy of the corresponding ECAL cluster, and the energy sum of all bremsstrahlung photons spatially compatible with originating from the electron track. The momentum of muons is obtained from

the curvature of the corresponding track. The energy of charged hadrons is determined from a combination of their momentum measured in the tracker (assuming the charged pion mass) and the matching ECAL and HCAL energy deposits, corrected for zero-suppression effects and for the response function of the calorimeters to hadronic showers. Finally, the energy of neutral hadrons is obtained from the corresponding corrected ECAL and HCAL energy.

A few sources of high-p_{T} muons from background processes need to be accounted for. These processes can be classified as reducible or irreducible. The reducible background includes muon decays that can be tagged and removed from the signal. These kind of events are mainly composed of $\mu^+\mu^-$ pairs from Drell-Yan decays ($\mathrm{Z}/\gamma*$) or high-p_{T} resonances, and high-p_{T} muons from jets produced through the strong interaction, referred to as QCD multijet events. The irreducible background sources comprise muon decays that can not be tagged event-by-event, and they are estimated using Monte Carlo (MC) simulations or data-driven techniques. The irreducible background include contributions from $\mathrm{Z}/\gamma* \to \tau\overline{\tau}$, $\mathrm{W} \to \tau\nu_\tau$ and $\mathrm{t} \to \mathrm{Wb}$, passing the analysis selection criteria described below.

To suppress the contribution from the reducible background sources, two criteria were used to select the events. First, muons are required to be isolated from nearby hadronic activity to reduce the jet background. Second, events containing at least two isolated oppositely charged muons, each with $p_{\mathrm{T}}^{\mu} > 15$ GeV/c, are removed, since they tend to originate from Drell-Yan or high-p_{T} resonance decays. The muon isolation (I_μ) is defined as the sum of the transverse momentum of all PF-reconstructed charged hadrons, neutral hadrons and photons, in a cone of radius $\mathrm{R} = \sqrt{(\Delta\eta)^2 + (\Delta\phi)^2} = 0.3$, where $\Delta\eta$ and $\Delta\phi$ are the pseudorapidity and azimuthal distances to the muon. A muon is considered isolated if I_μ is less than 15% of the muon p_{T}.

Another important characteristic of W boson semi-muonic decays is the production of neutrinos. Since neutrinos are not detected in CMS, their presence is characterized by a particle momentum imbalance in the transverse plane, called missing tranverse momemtum $p_{\mathrm{T}}^{\mathrm{miss}}$. The $p_{\mathrm{T}}^{\mathrm{miss}}$ is defined as the magnitude of the negative vector sum of the p_{T} of all reconstructed PF objects in an event. In this analysis, the $p_{\mathrm{T}}^{\mathrm{miss}}$ distribution is used to extract the signal yields in twenty-four muon η_{CM}^{μ} bins, each 0.2 units wide except for the most backward ($-2.86 < \eta_{\mathrm{CM}}^{\mu} < -2.6$, $-2.2 < \eta < -1.93$, $-1.93 < \eta_{\mathrm{CM}}^{\mu} < -1.8$), and forward ($1.8 < \eta_{\mathrm{CM}}^{\mu} < 1.93$) regions.

The shape of the QCD multijet background is modelled with a functional form described by a modified Rayleigh distribution defined as:

$$f\left(p_{\mathrm{T}}^{\mathrm{miss}}\right) = p_{\mathrm{T}}^{\mathrm{miss}} \exp\left[-\left(p_{\mathrm{T}}^{\mathrm{miss}}\right)^2 \Big/ 2\left(\sigma_0 + \sigma_1 p_{\mathrm{T}}^{\mathrm{miss}} + \sigma_2\left(p_{\mathrm{T}}^{\mathrm{miss}}\right)^2\right)^2\right] \quad (1)$$

It reproduces the $p_{\mathrm{T}}^{\mathrm{miss}}$ shape of data events containing nonisolated muons. The QCD shape is extracted by fitting the data in five relative muon isolation ($I_\mu / p_{\mathrm{T}}^{\mu}$) bins from 0.4 to 0.9. The σ_0, σ_1, and σ_2 parameters extracted from the fits are then linearly extrapolated to the isolated muon signal regime and the resulting function is used as the QCD multijet background shape.

The $p_{\mathrm{T}}^{\mathrm{miss}}$ distribution of the signal and electroweak backgrounds is described using templates from MC simulations. The MC samples were generated using the next-to-leading-order (NLO) generator POWHEG v2 [31–33]. In order to take into account electroweak (EWK) corrections, the POWHEG BOX packages `W_ew-BMMNP` [34] and `Z_ew-BMMNPV` [35] were used to generate the $\mathrm{pp} \to \mathrm{W} \to l\nu_{\mathrm{l}}$ and $\mathrm{pp} \to \mathrm{Z}/\gamma* \to l^+l^-$ processes, respectively. The $\mathrm{pp} \to \mathrm{t\bar{t}}$ decays were generated using the POWHEG BOX package `hvq` [36], which is a heavy flavor quark generator. The simulation of pPb collisions was performed using the CT14 [2] PDF corrected with the EPPS16 nuclear modification factors derived for Pb ions [24]. The parton densities of protons

and neutrons were scaled according to the mass and atomic number of the lead isotopes.

The parton showering was performed by hadronizing the events using PYTHIA 8.212 [37] with the CUETP8M1 underlying event (UE) tune [38, 39]. To consider a more realistic distribution of the underlying environment present in pPb collisions, the POWHEG samples were embedded in simulated pPb events generated by EPOS [40], taking into account the pPb boost. The EPOS simulation was tuned to reproduce the global event properties of the pPb data such as the pseudorapidity distributions of charged hadrons [41]. The embedding of the signal and pPb underlying events was performed requiring the same generated interaction point when simulating the detector hits. The trigger decisions were emulated and the embedded events were reconstructed with the same algorithms used for data. The detector response was simulated with GEANT4 [42].

The agreement between the electroweak simulations and the data is improved by weighing the electroweak boson p_{T} distribution using a p_{T}-dependent function derived from the ratio of the Z boson p_{T} distributions in $\mathrm{Z}/\gamma* \to \mu^+\mu^-$ events in data and simulation. Furthermore, the pPb event activity is reweighed by matching the simulated total energy distribution reconstructed in both sides of the HF calorimeters to the one observed in data in a $\mathrm{Z}/\gamma* \to \mu^+\mu^-$ sample.

Due to momentum conservation, the production of Z and W bosons is balanced by a hadronic recoil composed of jets and particles from the pPb underlying activity. The distribution of the hadronic recoil significantly contributes to the $p_{\mathrm{T}}^{\mathrm{miss}}$ resolution. Due to the similarity of the production process of Z and W bosons, and their similar masses, we assume that the recoil distributions are the same for both species. Therefore, the correction of the recoil distribution in MC is derived in a control region of $\mathrm{Z} \to \mu^+\mu^-$ events using the hadronic recoil technique [43]. The hadronic recoil of $\mathrm{Z} \to \mu^+\mu^-$ events, $\vec{u}_T$, is defined as the vector sum of the transverse momentum of all PF candidates excluding the decay products of the Z boson. The distributions of the hadronic recoil components parallel and perpendicular to the Z boson transverse momentum $\vec{p}_T^{\,Z}$ are fitted in MC and data using a weighed sum of two Gaussian functions. The mean and resolution values extracted from the recoil fits are used to scale the simulated hadronic recoil distributions to match the performance measured in data. The corrected $p_{\mathrm{T}}^{\mathrm{miss}}$ is then derived in the electroweak MC samples as the vector sum of $\vec{u}_T^{\,\mathrm{corr}}$ and the $\vec{p}_T$ of the reconstructed muons from the decay of Z and W bosons.

The number of $\mathrm{W} \to \mu\nu_\mu$ events is extracted by performing an unbinned log-likelihood fit of the observed $p_{\mathrm{T}}^{\mathrm{miss}}$ distribution in each muon η_{CM} bin. The $p_{\mathrm{T}}^{\mathrm{miss}}$ shapes assumed for the electroweak processes are based on POWHEG MC binned templates. The total fit model includes six contributions: the signal $\mathrm{W} \to \mu\nu_\mu$ template, the EWK backgrounds $\mathrm{Z}/\gamma* \to \mu^+\mu^-$, $\mathrm{W} \to \tau\nu_\tau$ and $\mathrm{Z}/\gamma* \to \tau\overline{\tau}$ templates, the $\mathrm{t\bar{t}}$ background template, and the QCD data-driven functional form. When fitting the data, the QCD shape parameters (σ_i) are fixed to the extrapolated values, while the ratio of the EWK background yields to the signal yield is fixed to the results from POWHEG. The observed numbers of muons coming from W boson decays over the entire η^{μ}_{CM} range are: 97971 ± 332 μ^+ and 81147 ± 301 μ^-, where the uncertainty is statistical, determined by the fit procedure. Examples of the resulting $p_{\mathrm{T}}^{\mathrm{miss}}$ distributions in the most central ($-0.2 < \eta^{\mu}_{\mathrm{CM}} < 0.0$) and forward ($1.8 < \eta^{\mu}_{\mathrm{CM}} < 1.93$) bins, are shown in Fig. 1, after applying all analysis corrections and selection criteria.

The simulated sample of $\mathrm{W} \to \mu\nu_\mu$ is used to derive the efficiency of the muon trigger, isolation, reconstruction, and selection criteria as a function of η^{μ}_{CM}. The individual components of the single muon efficiency are also directly estimated from pPb data in a $\mathrm{Z} \to \mu^+\mu^-$ sample using the Tag-and-Probe (TnP) technique, as described in Ref. [44]. The muon efficiencies computed from data are then compared to the corresponding muon efficiencies derived from the MC

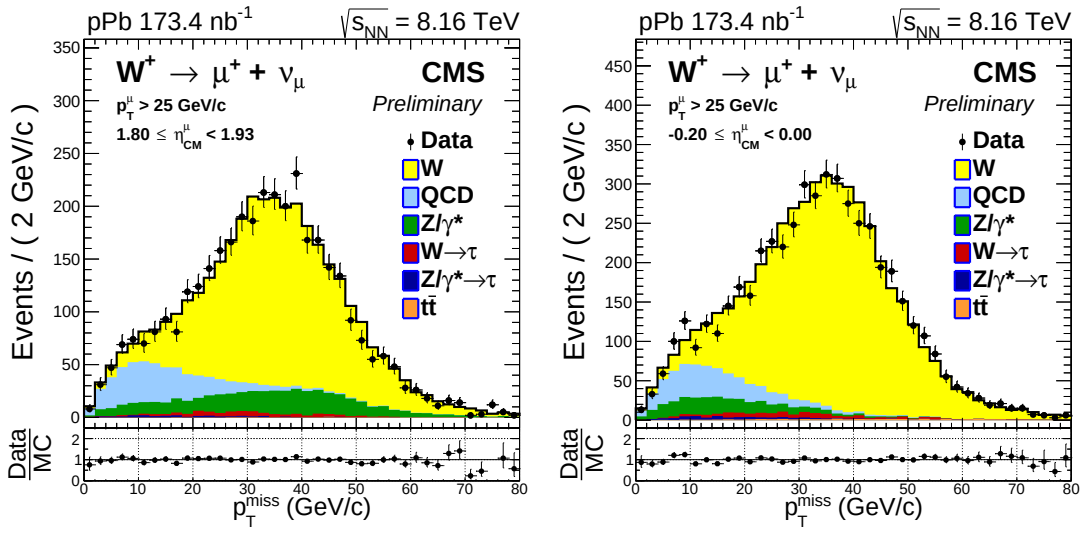

Figure 1: The missing transverse momentum $p_{\mathrm{T}}^{\mathrm{miss}}$ distribution for $\mathrm{W}^{+} \to \mu^{+}\nu_{\mu}$ events within the $-0.2 < \eta_{\mathrm{CM}}^{\mu} < 0.0$ (left) and $1.8 < \eta_{\mathrm{CM}}^{\mu} < 1.93$ (right) ranges. Unbinned fits to the data (black points) are performed with six contributions, stacked from bottom to top: $\mathrm{t\bar{t}}$ (orange), $\mathrm{Z}/\gamma* \to \tau\overline{\tau}$ (dark blue), $\mathrm{W}^{+} \to \overline{\tau}\nu_{\tau}$ (red), $\mathrm{Z}/\gamma* \to \mu^{+}\mu^{-}$ (green), QCD multijet (light blue) and $\mathrm{W}^{+} \to \mu^{+}\nu_{\mu}$ (yellow). The η_{CM}^{μ} regions are defined such that the proton is moving towards positive pseudorapidity. Error bars represent statistical uncertainties. The lower panels display the data divided by the result of the fit, for each $p_{\mathrm{T}}^{\mathrm{miss}}$ bin.

samples. The reconstruction efficiency is observed to be consistent while the trigger efficiency is lower in the Z simulation by 5% than in data at $|\eta_{\mathrm{lab}}^{\mu}| = 1.4$. The muon isolation selection is found to reject less muons in the simulation, due to the lower pPb underlying event activity present compared to data. In order to correct the differences between data and simulation, the muon efficiency computed from the $\mathrm{W} \to \mu\nu_{\mu}$ MC sample is multiplying by the TnP scale factors event-by-event. The correction factors are computed, in bins of muon p_{T}^{μ} and η_{lab}, from the ratio of the muon efficiencies measured in data to those calculated from simulations in $\mathrm{Z} \to \mu^{+}\mu^{-}$ events. The TnP scale factors change the muon efficiency from -3% in the mid-rapidity region ($|\eta_{\mathrm{lab}}^{\mu}| < 1.0$) to $+5\%$ at $\eta_{\mathrm{lab}}^{\mu} = 1.4$. The TnP corrected efficiencies vary with η_{CM}^{μ}, from $(81 \pm 1)\%$ to $(92 \pm 2)\%$.

The leading source of systematic uncertainty originates from the efficiency TnP corrections. The uncertainties of the TnP corrections are determined by propagating the uncertainties of the muon efficiencies extracted from data and simulation, derived from the fits to the invariant mass of $\mathrm{Z} \to \mu^{+}\mu^{-}$ candidates. These uncertainties comprise a statistical component due to the finite size of the data sample available, as well as a systematic component estimated from variations in the fitting procedure. Additionally, an uncertainty to account for the possible differences in the reconstruction of muon tracks of 0.6% and an uncertainty of 0.34% to account for the impact of pileup and underlying event activity, are included. Another important source of systematic uncertainty arises from the modeling of the QCD multijet $p_{\mathrm{T}}^{\mathrm{miss}}$ distribution in the signal region, which is estimated by letting the QCD shape parameters vary within the RMS of the extrapolated values in bins of η_{CM}^{μ}, and by changing the $p_{\mathrm{T}}^{\mathrm{miss}}$ model to the one used in Ref. [12].

The uncertainty on the normalization of the electroweak background is estimated from the nPDF uncertainty on the Z over W boson inclusive cross sections (according to CT14+EPPS16), the uncertainty on the W and Z bosons branching fractions to leptons [45], and the experimen-

tal uncertainty on the ttbar cross section in pPb [29]. The uncertainty on the vector boson p_{T} reweighing is derived from the difference with respect to not applying the boson p_{T} correction. The uncertainty on the binning of the $p_{\mathrm{T}}^{\mathrm{miss}}$ MC templates is estimated by changing to a $p_{\mathrm{T}}^{\mathrm{miss}}$ bin size of 1 GeV/c. The impact of electroweak corrections in POWHEG is estimated from the difference in the efficiency when computed using POWHEG without electroweak corrections [46]. The uncertainty on the $p_{\mathrm{T}}^{\mathrm{miss}}$ recoil correction is determined by changing the model used to fit the hadronic recoil distribution and the profile of the recoil mean and resolution as a function of the p_{T}^{Z}. And finally, the mismodelling of the underlying event activity in the simulations is estimated by reweighing the distribution of the track multiplicity instead of the energy deposited in the HF calorimeters. The integrated luminosity measurement uncertainty (5.0%) only affects the W boson differential cross sections and cancels in the asymmetry measurements. The maximum relative uncertainty of the differential cross sections and absolute uncertainties of the asymmetries are presented for each systematic category in Table 1.

Table 1: Maximum uncertainty of the measured observables as a function of η_{CM}^{μ} determined for each category. The uncertainties of the cross sections are relative while for the asymmetries are absolute. The global luminosity uncertainty of $\pm$5.0% is not included in the total systematic uncertainty of the cross sections.

Category	$\mathrm{W}^{-}d\sigma/d\eta_{CM}$ [%]	$\mathrm{W}^{+}d\sigma/d\eta_{CM}$ [%]	$\mathrm{W}^{-}R_{FB}$	$\mathrm{W}^{+}R_{FB}$	$\mathrm{W}R_{FB}$	$(N_{\mu}^{+}-N_{\mu}^{-})/(N_{\mu}^{+}+N_{\mu}^{-})$
Boson p_{T} reweighing	0.5	0.4	0.001	0.001	0.001	0.001
EWK background	0.4	0.3	0.002	0.001	0.001	0.000
POWHEG EWK correction	0.9	0.5	0.007	0.004	0.006	0.003
Efficiency	3.0	3.2	0.026	0.037	0.030	0.011
Event activity reweighing	0.6	0.4	0.002	0.002	0.001	0.002
MET template binning	0.1	0.1	0.002	0.001	0.001	0.001
QCD background	1.2	0.7	0.016	0.007	0.009	0.006
Hadronic recoil correction	0.2	0.3	0.002	0.004	0.002	0.002
Total systematic uncertainty	3.3	3.3	0.030	0.038	0.031	0.013
Statistical uncertainy	2.4	2.0	0.026	0.029	0.019	0.015

3 Results

The W boson differential cross sections are computed as a function of η_{CM}^{μ}, requiring muons of $p_{\mathrm{T}} > 25\,\mathrm{GeV}/c$. The differential $\mathrm{W} \to \mu\nu_{\mu}$ cross sections are determined from

$$\frac{d\sigma(\mathrm{W} \to \mu\nu_{\mu})}{d\eta_{\mathrm{CM}}^{\mu}}\left(\eta_{\mathrm{CM}}^{\mu}\right) = \frac{N_{\mu}\left(\eta_{\mathrm{CM}}^{\mu}\right)}{\mathcal{L}\Delta\eta_{\mathrm{CM}}^{\mu}}$$

where N_{μ} is the efficiency-corrected muon yield, $\mathcal{L}$ is the recorded integrated luminosity, and $\Delta\eta_{\mathrm{CM}}^{\mu}$ is the width of the measured bin.

The cross sections for the positive and negative $\mathrm{W} \to \mu\nu_{\mu}$ decays are compared in Fig. 2 with NLO perturbative QCD predictions calculated with the Monte Carlo program MCFM [47] using the CT14 [2] proton PDF. In addition, two calculations include nuclear modifications in the PDF, given by nCTEQ15 [48] and EPPS16 [24] nPDF sets (labelled as CT14+nCTEQ15 and CT14+EPPS16, respectively). The nPDF uncertainties are propagated in the standard way for Hessian nPDF sets as prescribed in Ref. [1]. As can be seen in Fig. 2, the predicted CT14+nCTEQ15 and CT14+EPPS16 cross sections are systematically below the calculation using CT14 PDF at

large positive muon rapidity, because of the depletion of the antiquark PDF in nuclei at small $x = M_W/\sqrt{s_{NN}} \times \exp(-y_W) \simeq M_W/\sqrt{s_{NN}} \times \exp(-\eta^{\mu}_{CM}) \sim 10^{-3}$. Conversely, calculations including nPDF modifications turn out to be above those using CT14 PDF in the negative rapidity region, due to the slight quark anti-shadowing at large $x \sim 0.1$. When compared to data, all theory calculations reproduce the measurement at backward rapidity, while at forward rapidity the calculations including nPDF effects appear to be favored.

In order to fully exploit the information provided by the data, two additional set of observables are measured: the muon charge asymmetry and the muon forward-backward ratios. The measurement of asymmetries has several advantages compared to the cross sections. First, they are more sensitive to the modifications of the quark PDFs [7]. Moreover, part of the theoretical and experimental uncertainties in the cross section measurements, such as that of the integrated luminosity or the theoretical scale dependence, cancel in these asymmetries.

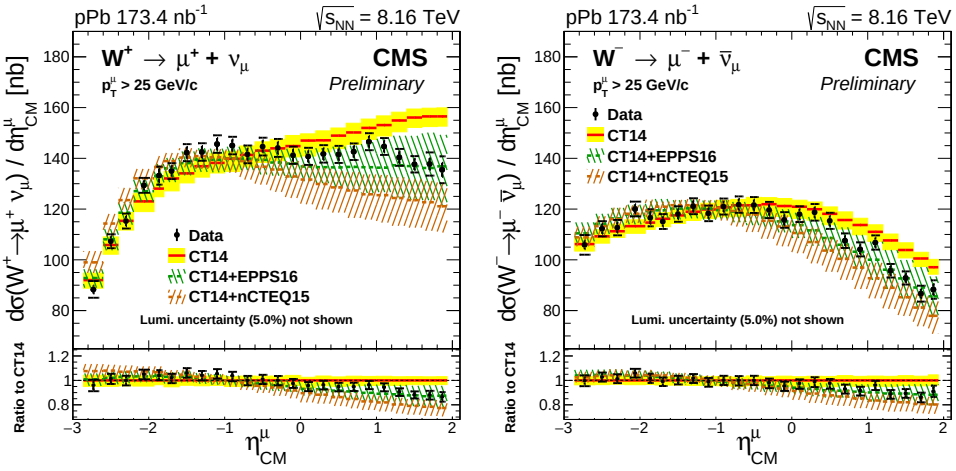

Figure 2: Production cross sections for $W^+ \to \mu^+\nu_\mu$ (left) and $W^- \to \mu^-\overline{\nu}_\mu$ (right), as a function of the muon pseudorapidity in the center-of-mass frame. The brackets represent the statistical and systematic uncertainties summed in quadrature, while the error bars show the statistical uncertainties only. The global luminosity uncertainty of ±5.0% is not shown. Calculations using with CT14 PDF (red line), CT14+EPPS16 nPDF (green line) and CT14+nCTEQ15 nPDF (brown line), are also displayed, including their PDF uncertainty bands at 68% confidence interval. The bottom panels show the ratio of data (black points), CT14+EPPS16 (green line) and CT14+nCTEQ15 (brown line) with respect to CT14.

The muon forward-backward ratios, defined as $N^{\pm}_{\mu}(+\eta^{\mu}_{CM})/N^{\pm}_{\mu}(-\eta^{\mu}_{CM})$ for both positive and negative muons, are compared in Fig. 3 to the CT14 PDF, CT14+EPPS16 nPDF and CT14+nCTEQ15 nPDF calculations. The results of both charged muons favor the predictions including nuclear modifications over the free-proton PDF calculations. Given the precision of the experimental results, the measurements provide constraints to both the CT14+EPPS16 and CT14+nCTEQ15 nPDF sets.

The yields of positive and negative charged muons are further combined to measure the forward-backward ratio of all muons $N_{\mu}(+\eta^{\mu}_{CM})/N_{\mu}(-\eta^{\mu}_{CM})$. This ratio probes the small-x nuclear modifications of the quark PDFs over the large-x nuclear modifications in the Pb nucleus. The results of this asymmetry are presented in Fig. 4, and they strongly deviate from the CT14 PDF predictions, favoring the CT14+nCTEQ15 and CT14+EPPS16 nPDF sets. Moreover, the experimental uncertainties turn out to be significantly smaller than the nPDF uncertainties. Consequently, these measurements could constrain the quark and antiquark distributions in nuclei, and will be valuable inputs for global fits to the data.

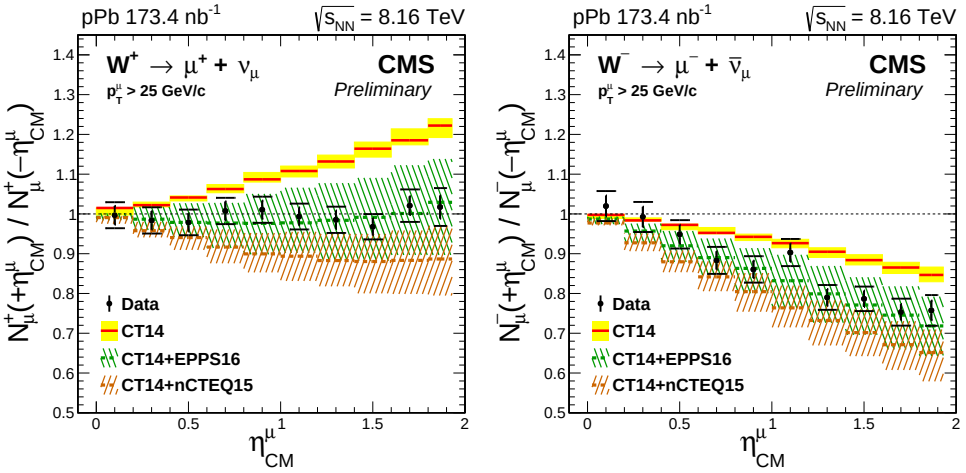

Figure 3: Forward-backward ratios, $N_\mu(+\eta^\mu_{\rm CM})/N_\mu(-\eta^\mu_{\rm CM})$, for the positive (left) and negative (right) muons. The brackets represent the statistical and systematic uncertainties summed in quadrature, while the error bars show the statistical uncertainties only. Calculations using with CT14 PDF (red line), CT14+EPPS16 nPDF (green line) and CT14+nCTEQ15 nPDF (brown line), are also displayed, including their PDF uncertainty bands at 68% confidence interval.

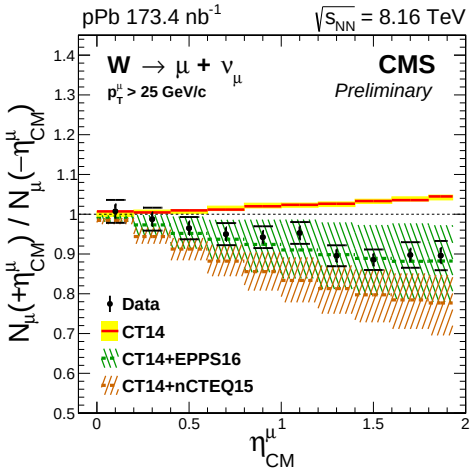

Figure 4: The forward-backward ratio of all muons, $N_\mu(+\eta^\mu_{\rm CM})/N_\mu(-\eta^\mu_{\rm CM})$, as a function of $\eta^\mu_{\rm CM}$. The brackets represent the statistical and systematic uncertainties summed in quadrature, while the error bars show the statistical uncertainties only. Calculations using with CT14 PDF (red line), CT14+EPPS16 nPDF (green line) and CT14+nCTEQ15 nPDF (brown line), are also displayed, including their PDF uncertainty bands at 68% confidence interval.

The muon charge asymmetry, defined as $\mathcal{A} \equiv (N_\mu^+ - N_\mu^-)/(N_\mu^+ + N_\mu^-)$, reflects the differences in the production of W^+ and W^- bosons. Fig. 5 shows the results of the muon charge asymmetry as a function of $\eta^\mu_{\rm CM}$, compared to the MCFM predictions calculated using CT14 PDF only and including nuclear modifications described by the EPPS16 and nCTEQ15 nPDFs. All calculations reproduce the present measurements in the entire muon pseudorapidity range. In particular, the discrepancy between data and theory reported at negative muon pseudorapidity in pPb collisions at $\sqrt{s_{\rm NN}} = 5.02\,\text{TeV}$ [12] is not observed in the present measurements. It should be noted that the present use of the CT14 proton PDF set decreases the value of the charge asymmetry compared to the predictions based on CT10 in Ref. [12]. Moreover, the theoretical uncertainties are also enlarged in the EPPS16 nPDF sets, as compared to the EPS09 nPDF sets used in the analysis at $\sqrt{s_{\rm NN}} = 5.02\,\text{TeV}$. It has been shown in Ref. [49] that the measure-

ments of the lepton charge asymmetry at different collision energies are simply related by a shift in the lepton pseudorapidity, $\mathcal{A}(\eta_\ell, \sqrt{s'}) = \mathcal{A}(\eta_\ell \pm \ln(\sqrt{s'}/\sqrt{s}), \sqrt{s})$. Following this procedure, it has been checked in Fig. 6 that the present results and the measurements performed at $\sqrt{s_{\mathrm{NN}}} = 5.02$ TeV [12] obey well this scaling property.

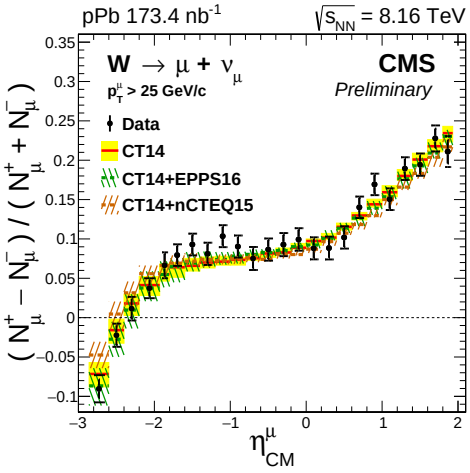

Figure 5: Muon charge asymmetry, $(N_\mu^+ - N_\mu^-)/(N_\mu^+ + N_\mu^-)$, as a function of the muon pseudorapidity in the center-of-mass frame. The brackets represent the statistical and systematic uncertainties summed in quadrature, while the error bars show the statistical uncertainties only. Calculations using with CT14 PDF (red line), CT14+EPPS16 nPDF (green line) and CT14+nCTEQ15 nPDF (brown line), are also displayed, including their PDF uncertainty bands at 68% confidence interval.

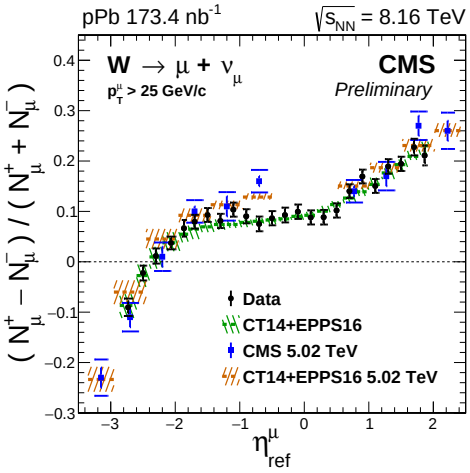

Figure 6: Comparison of the muon charge asymmetry measured at 8.16 TeV (black points) and at 5.02 TeV [12] (blue squares). The muon pseudorapidity has been shifted according to $\eta^\mu_{\mathrm{ref}} = \eta^\mu_{\mathrm{CM}} \pm \ln\left(8.16\ \mathrm{TeV}/\sqrt{s_{\mathrm{NN}}}\right)$. The brackets represent the statistical and systematic uncertainties summed in quadrature, while the error bars show the statistical uncertainties only. Calculations using with CT14+EPPS16 nPDF at 8.16 TeV (green line) and at 5.02 TeV (brown line), are also displayed, including their PDF uncertainty bands at 68% confidence interval.

The agreement between data and theory calculations is quantified through a χ^2 test performed for each observable taking into account the bin-to-bin correlations of both experimental and theoretical uncertainties. The results of the χ^2 test and the number of degrees of freedom (ndf) of each observable are shown in Table 2. The CT14+EPPS16 and CT14+nCTEQ15 nPDF predictions prove compatible with the data, while the CT14 PDF calculations do not describe well

the measurements. These experimental results thus provide for the first time a clear evidence of the nuclear modification of quark PDF from the measurements of weak boson production in nuclear collisions.

Table 2: Results of the χ^2 statistical test between the measurements and the theory calculations from the CT14 PDF, CT14+EPPS16 nPDF and CT14+nCTEQ15 nPDF calculations. The value of the χ^2, the number of degrees of freedom (ndf) and the χ^2 probability (Prob.), are presented for the W differential cross sections, the muon charge asymmetry, the charged muon forward-backward ratios, and the forward-backward ratio of all muons, respectively.

Observable	CT14			CT14+EPPS16			CT14+nCTEQ15		
	χ^2	ndf	Prob.(%)	χ^2	ndf	Prob.(%)	χ^2	ndf	Prob.(%)
$d\sigma(\mathrm{W} \to \mu\nu_\mu)/d\eta^\mu_{\mathrm{CM}}$	135	48	3×10^{-8}	32	48	96	40	48	79
$(N^+_\mu - N^-_\mu)/(N^+_\mu + N^-_\mu)$	23	24	54	18	24	80	29	24	23
$N^\pm_\mu(+\eta^\mu_{\mathrm{CM}})/N^\pm_\mu(-\eta^\mu_{\mathrm{CM}})$	98	20	3×10^{-10}	11	20	95	14	20	83
$N_\mu(+\eta^\mu_{\mathrm{CM}})/N_\mu(-\eta^\mu_{\mathrm{CM}})$	87	10	2×10^{-12}	3	10	99	5	10	90

Further, the possible sources of differences between data and the (n)PDFs are investiged. In the Hessian representation, a central PDF is given along with error sets, each of which corresponds to an eigenvector of the covariance matrix in parameter space [50]. The values of χ^2/ndf between the absolute cross sections and the calculations using each of these individual sets of CT14, nCTEQ15 and EPPS16 (57, 33 and 41 error sets, respectively) have been determined. Fig. 7 shows the distribution of the χ^2/ndf values for the central and error sets. While most of the EPPS16 individual sets lead to a good agreement with data (with χ^2/ndf of order unity), only those nCTEQ15 sets which exhibit the smaller quark shadowing at small x are compatible with the data shown in this analysis. All CT14 sets without nPDF modification lead to a narrow distribution centered around $\chi^2/\mathrm{ndf} \simeq 3$. The current measurements of W production in pPb collisions will permit further constraints the quark and antiquark nPDF and the amount of quark shadowing in nuclei.

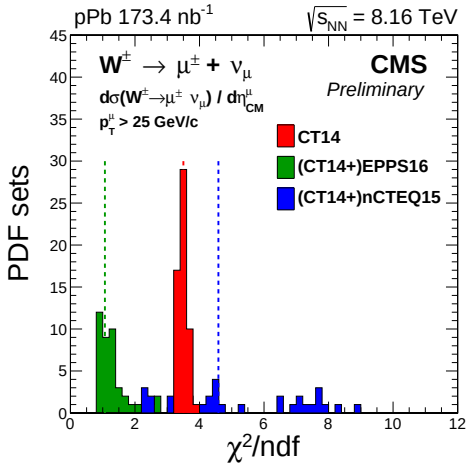

Figure 7: Distribution of the χ^2/ndf values from the comparison of data (absolute cross sections) and theoretical calculations, for the CT14, nCTEQ15 and EPPS16 individual sets. The vertical dashed lines represent the prediction corresponding to the central set of CT14, nCTEQ15, and EPPS16.

4 Summary

A measurement of W boson production in pPb collisions at $\sqrt{s_{\mathrm{NN}}} = 8.16\,\mathrm{TeV}$ is reported, using the muon decay channel for muons with p_{T} greater than 25 GeV/c and $|\eta_{\mathrm{lab}}| < 2.4$. The absolute differential production cross sections for positive and negative $\mathrm{W} \to \mu\nu_{\mu}$ decays, the muon charge asymmetry and the muon forward-backward ratios, are measured as a function of the muon pseudorapidity in the center-of-mass frame, in the range $\eta^{\mu}_{\mathrm{CM}} \in [-2.86, 1.93]$.

The measurements are compared to theoretical predictions assuming both proton PDF (CT14) and nuclear PDF (CT14+EPPS16 , CT14+nCTEQ15) sets. The absolute cross sections and the forward-backward asymmetries exhibit significant deviations from the CT14 case, revealing nuclear modifications of the PDFs unambiguously for the first time in the production of weak bosons in nuclear collisions. On the contrary, both the CT14+EPPS16 and the CT14+nCTEQ15 calculations show a good overall agreement with data, though the data favors the former global fit. In the latter case, nevertheless, only the individual sets which exhibit the smallest nuclear PDF modifications at small values of x (in the shadowing region) turn out to be compatible with experimental measurements. The small experimental uncertainties reported in the measurements will enable a significant reduction of the current uncertainties of the quark and antiquark nPDFs, in the range $10^{-3} \lesssim x \lesssim 10^{-1}$.

References

[1] J. Butterworth et al., "PDF4LHC recommendations for LHC Run II", *Journal of Physics G: Nuclear and Particle Physics* **43** (2016) 023001, doi:10.1088/0954-3899/43/2/023001, arXiv:1510.03865.

[2] S. Dulat et al., "New parton distribution functions from a global analysis of quantum chromodynamics", *Phys. Rev. D* **93** (2016) 033006, doi:10.1103/PhysRevD.93.033006, arXiv:1506.07443.

[3] NNPDF Collaboration, "Parton distributions for the LHC Run II", *JHEP* **04** (2015) 040, doi:10.1007/JHEP04(2015)040, arXiv:1410.8849.

[4] L. A. Harland-Lang, A. D. Martin, P. Motylinski, and R. S. Thorne, "Parton distributions in the LHC era: MMHT 2014 PDFs", *Eur. Phys. J. C* **75** (2015) 204, doi:10.1140/epjc/s10052-015-3397-6, arXiv:1412.3989.

[5] R. Vogt, "Shadowing effects on vector boson production", *Phys. Rev. C* **64** (2001) 044901, doi:10.1103/PhysRevC.64.044901, arXiv:hep-ph/0011242.

[6] X.-F. Zhang and G. I. Fai, "Z^0 production as a test of nuclear effects at the LHC", *Phys. Lett. B* **545** (2002) 91, doi:10.1016/S0370-2693(02)02558-3, arXiv:hep-ph/0205155.

[7] H. Paukkunen and C. A. Salgado, "Constraints for the nuclear parton distributions from Z and W production at the LHC", *JHEP* **03** (2011) 071, doi:10.1007/JHEP03(2011)071, arXiv:1010.5392.

[8] N. Armesto, "Nuclear shadowing", *J. Phys. G* **32** (2006) R367, doi:10.1088/0954-3899/32/11/R01, arXiv:hep-ph/0604108.

[9] CDF Collaboration, "Direct Measurement of the W Production Charge Asymmetry in $\mathrm{p\overline{p}}$ Collisions at $\sqrt{s} = 1.96$ TeV", *Phys. Rev. Lett.* **102** (2009) 181801, doi:10.1103/PhysRevLett.102.181801, arXiv:0901.2169.

[10] CMS Collaboration, "Measurement of the muon charge asymmetry in inclusive pp $\to W + X$ production at $\sqrt{s} = 7$ TeV and an improved determination of light parton distribution functions", *Phys. Rev. D* **90** (2014) 032004, doi:10.1103/PhysRevD.90.032004, arXiv:1312.6283.

[11] CMS Collaboration, "Measurement of the electron charge asymmetry in inclusive W production in pp collisions at $\sqrt{s} = 7$ TeV", *Phys. Rev. Lett.* **109** (2012) 111806, doi:10.1103/PhysRevLett.109.111806, arXiv:1206.2598.

[12] CMS Collaboration, "Study of W boson production in pPb collisions at $\sqrt{s_{\mathrm{NN}}} = 5.02$ TeV", *Phys. Lett. B* **750** (2015) 565, doi:10.1016/j.physletb.2015.09.057, arXiv:1503.05825.

[13] Z. Conesa del Valle et al., "Effect of heavy-quark energy loss on the muon differential production cross-section in Pb-Pb collisions at $\sqrt{s_{\mathrm{NN}}} = 5.5$ TeV", *Phys. Lett. B* **663** (2008) 202, doi:10.1016/j.physletb.2008.03.073, arXiv:0712.0051.

[14] Z. Conesa del Valle, "Vector bosons in heavy-ion collisions at the LHC", *Eur. Phys. J. C* **61** (2009) 729, doi:10.1140/epjc/s10052-009-0980-8, arXiv:0903.1432.

[15] ATLAS Collaboration, "Measurement of the centrality dependence of J/ψ yields and observation of Z production in lead-lead collisions with the ATLAS detector at the LHC", *Phys. Lett. B* **697** (2011) 294, doi:10.1016/j.physletb.2011.02.006, arXiv:1012.5419.

[16] ATLAS Collaboration, "Measurement of Z boson Production in PbPb Collisions at $\sqrt{s_{\mathrm{NN}}} = 2.76$ TeV with the ATLAS Detector", *Phys. Rev. Lett.* **110** (2013) 022301, doi:10.1103/PhysRevLett.110.022301, arXiv:1210.6486.

[17] ATLAS Collaboration, "Measurement of the production and lepton charge asymmetry of W bosons in Pb+Pb collisions at $\sqrt{s_{\mathrm{NN}}} = 2.76$ TeV with the ATLAS detector", *Eur. Phys. J. C* **75** (2015) 23, doi:10.1140/epjc/s10052-014-3231-6, arXiv:1408.4674.

[18] CMS Collaboration, "Study of Z boson production in PbPb collisions at nucleon-nucleon centre of mass energy = 2.76 TeV", *Phys. Rev. Lett.* **106** (2011) 212301, doi:10.1103/PhysRevLett.106.212301, arXiv:1102.5435.

[19] CMS Collaboration, "Study of Z production in PbPb and pp collisions at $\sqrt{s_{\mathrm{NN}}} = 2.76$ TeV in the dimuon and dielectron decay channels", *JHEP* **03** (2015) 022, doi:10.1007/JHEP03(2015)022, arXiv:1410.4825.

[20] CMS Collaboration, "Study of W boson production in PbPb and pp collisions at $\sqrt{s_{NN}} = 2.76$ TeV", *Phys. Lett. B* **715** (2012) 66, doi:10.1016/j.physletb.2012.07.025, arXiv:1205.6334.

[21] ATLAS Collaboration, "Measurement of $W \to \mu\nu$ production in p+Pb collision at $\sqrt{s_{\mathrm{NN}}} = 5.02$ TeV with ATLAS detector at the LHC", Technical Report ATLAS-CONF-2015-056, 2015.

[22] ALICE Collaboration, "W and Z boson production in p-Pb collisions at $\sqrt{s_{\mathrm{NN}}}$ = 5.02 TeV", *JHEP* **02** (2017) 077, doi:10.1007/JHEP02(2017)077, arXiv:1611.03002.

[23] CMS Collaboration, "Study of Z boson production in pPb collisions at $\sqrt{s_{NN}} = 5.02$ TeV", *Phys. Lett. B* **759** (2016) 36, doi:10.1016/j.physletb.2016.05.044, arXiv:1512.06461.

[24] K. J. Eskola, P. Paakkinen, H. Paukkunen, and C. A. Salgado, "EPPS16: Nuclear parton distributions with LHC data", *Eur. Phys. J. C* **77** (2017) 163, doi:10.1140/epjc/s10052-017-4725-9, arXiv:1612.05741.

[25] CMS Collaboration, "The CMS experiment at the CERN LHC", *JINST* **3** (2008) S08004, doi:10.1088/1748-0221/3/08/S08004.

[26] E. Todesco and J. Wenninger, "Large Hadron Collider momentum calibration and accuracy", *Phys. Rev. Accel. Beams* **20** (2017) 081003, doi:10.1103/PhysRevAccelBeams.20.081003.

[27] CMS Collaboration, "The CMS trigger system", *JINST* **12** (2017) P01020, doi:10.1088/1748-0221/12/01/P01020, arXiv:1609.02366.

[28] CMS Collaboration, "Performance of CMS muon reconstruction in pp collision events at $\sqrt{s} = 7$ TeV", *JINST* **7** (2012) P10002, doi:10.1088/1748-0221/7/10/P10002, arXiv:1206.4071.

[29] CMS Collaboration, "Observation of top quark production in proton-nucleus collisions", *Phys. Rev. Lett.* **119** (2017) 242001, doi:10.1103/PhysRevLett.119.242001, arXiv:1709.07411.

[30] CMS Collaboration, "Particle-flow reconstruction and global event description with the CMS detector", *JINST* **12** (2017) P10003, doi:10.1088/1748-0221/12/10/P10003, arXiv:1706.04965.

[31] S. Frixione, P. Nason, and C. Oleari, "Matching NLO QCD computations with parton shower simulations: the POWHEG method", *JHEP* **11** (2007) 070, doi:10.1088/1126-6708/2007/11/070, arXiv:0709.2092.

[32] P. Nason, "A new method for combining NLO QCD with shower Monte Carlo algorithms", *JHEP* **11** (2004) 040, doi:10.1088/1126-6708/2004/11/040, arXiv:hep-ph/0409146.

[33] S. Alioli, P. Nason, C. Oleari, and E. Re, "A general framework for implementing NLO calculations in shower Monte Carlo programs: the POWHEG BOX", *JHEP* **06** (2010) 043, doi:10.1007/JHEP06(2010)043, arXiv:1002.2581.

[34] L. Barze et al., "Implementation of electroweak corrections in the POWHEG BOX: single W production", *JHEP* **04** (2012) 037, doi:10.1007/JHEP04(2012)037, arXiv:1202.0465.

[35] L. Barze et al., "Neutral-current Drell–Yan with combined QCD and electroweak corrections in the POWHEG BOX", *Eur. Phys. J. C* **73** (2013) 2474, doi:10.1140/epjc/s10052-013-2474-y, arXiv:1302.4606.

[36] S. Frixione, P. Nason, and G. Ridolfi, "A positive-weight next-to-leading-order Monte Carlo for heavy flavour hadroproduction", *JHEP* **09** (2007) 126, doi:10.1088/1126-6708/2007/09/126, arXiv:0707.3088.

[37] T. Sjöstrand et al., "An Introduction to PYTHIA 8.2", *Comput. Phys. Commun.* **191** (2015) 159, doi:10.1016/j.cpc.2015.01.024, arXiv:1410.3012.

[38] CMS Collaboration, "Event generator tunes obtained from underlying event and multiparton scattering measurements", *Eur. Phys. J. C* **76** (2016) 155, doi:10.1140/epjc/s10052-016-3988-x, arXiv:1512.00815.

[39] CMS Collaboration, "Study of the underlying event at forward rapidity in pp collisions at $\sqrt{s}$ = 0.9, 2.76, and 7 TeV", *JHEP* **04** (2013) 072, doi:10.1007/JHEP04(2013)072, arXiv:1302.2394.

[40] T. Pierog et al., "EPOS LHC: Test of collective hadronization with data measured at the CERN Large Hadron Collider", *Phys. Rev. C* **92** (2015) 034906, doi:10.1103/PhysRevC.92.034906, arXiv:1306.0121.

[41] CMS Collaboration, "Pseudorapidity distributions of charged hadrons in proton-lead collisions at $\sqrt{s_{\mathrm{NN}}} = 5.02$ and 8.16 TeV", *JHEP* **01** (2018) 045, doi:10.1007/JHEP01(2018)045, arXiv:1710.09355.

[42] GEANT4 Collaboration, "GEANT4: A Simulation toolkit", *Nucl. Instrum. Meth. A* **506** (2003) 250, doi:10.1016/S0168-9002(03)01368-8.

[43] CMS Collaboration, "Missing transverse energy performance of the CMS detector", *JINST* **6** (2011) P09001, doi:10.1088/1748-0221/6/09/P09001, arXiv:1106.5048.

[44] CMS Collaboration, "Measurements of Inclusive W and Z Cross Sections in pp Collisions at $\sqrt{s} = 7$ TeV", *JHEP* **01** (2011) 080, doi:10.1007/JHEP01(2011)080, arXiv:1012.2466.

[45] Particle Data Group Collaboration, "Review of Particle Physics", *Chin. Phys. C* **40** (2016) 100001, doi:10.1088/1674-1137/40/10/100001.

[46] S. Alioli, P. Nason, C. Oleari, and E. Re, "NLO vector-boson production matched with shower in POWHEG", *JHEP* **07** (2008) 060, doi:10.1088/1126-6708/2008/07/060, arXiv:0805.4802.

[47] R. Boughezal et al., "Color singlet production at NNLO in MCFM", *Eur. Phys. J. C* **77** (2017) 7, doi:10.1140/epjc/s10052-016-4558-y, arXiv:1605.08011.

[48] K. Kovařík et al., "nCTEQ15: Global analysis of nuclear parton distributions with uncertainties in the CTEQ framework", *Phys. Rev. D* **93** (Apr, 2016) 085037, doi:10.1103/PhysRevD.93.085037, arXiv:1509.00792.

[49] F. Arleo, É. Chapon, and H. Paukkunen, "Scaling properties of inclusive $W^{\pm}$ production at hadron colliders", *Eur. Phys. J. C* **76** (2016) 214, doi:10.1140/epjc/s10052-016-4049-1, arXiv:1509.03993.

[50] J. Pumplin et al., "Uncertainties of predictions from parton distribution functions. 2. The Hessian method", *Phys. Rev. D* **65** (2001) 014013, doi:10.1103/PhysRevD.65.014013, arXiv:hep-ph/0101032.